Elucidating the Structural Chemistry of a Hysteretic Iron(II) Spin-Crossover Compound From its Copper(II) and Zinc(II) Congeners

Christopher M. Pask,[a] Sam Greatorex,[a] Rafal Kulmaczewski,[a] Amgalanbaatar Baldansuren,[b,c] Eric J. L. McInnes,[b] Faith Bamiduro,[d] Mihoko Yamada,[e,f] Nobuto Yoshinari,[e] Takumi Konno[e] and Malcolm A. Halcrow*[a,e]

Abstract: Annealing [FeL_2][BF$_4$]$_2$·2H$_2$O (L = 2,6-*bis*-[5-methyl-1*H*-pyrazol-3-yl]pyridine) affords an anhydrous material, which undergoes a spin-transition at $T_{1/2}$ = 205 K with a 65 K thermal hysteresis loop. This occurs *via* a sequence of phase changes, which were monitored by powder diffraction in an earlier study. [CuL_2][BF$_4$]$_2$·2H$_2$O and [ZnL_2][BF$_4$]$_2$·2H$_2$O are not perfectly isostructural but, unlike the iron compound, they undergo single-crystal-to-single-crystal dehydration upon annealing. All the annealed compounds initially adopt the same tetragonal phase, but undergo a phase change near room temperature upon recooling. The low-temperature phase of [CuL_2][BF$_4$]$_2$ involves ordering of its Jahn-Teller distortion, to a monoclinic lattice with three unique cation sites. The zinc compound adopts a different, triclinic low-temperature phase with significant twisting of its coordination sphere, which unexpectedly becomes more pronounced as the crystal is cooled. Synchrotron powder diffraction data confirm the structural changes in the anhydrous zinc complex are reproduced in the high-spin iron compound, before the onset of spin-crossover. This will contribute to the wide hysteresis in the spin transition of the iron complex. EPR spectra of copper-doped [Fe$_{0.97}$Cu$_{0.03}L_2$][BF$_4$]$_2$ imply its low spin phase contains two distinct cation environments in a 2:1 ratio.

[a]   Dr. C. M. Pask, Dr. S. Greatorex, Dr. R. Kulmaczewski,
        Prof. M. A. Halcrow
        School of Chemistry, University of Leeds, Woodhouse Lane, Leeds,
        LS2 9JT (UK).
        E-mail: m.a.halcrow@leeds.ac.uk
        Homepage: http://www.chem.leeds.ac.uk/People/Halcrow.html
[b]   Dr. A. Baldansuren, Prof. E. J. L. McInnes
        School of Chemistry and Photon Science Institute, University of
        Manchester, Oxford Road, Manchester M13 9PL (UK).
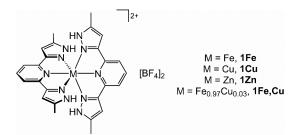[c]   Dr. A. Baldansuren, current address:
        Chemistry and Chemical Biology, 120 Cogswell, Rensselaer
        Polytechnic Institute, 110 Eighth Street, Troy, NY 12180, USA.
[d]   Dr. F. Bamiduro
        School of Chemical and Process Engineering, University of Leeds,
        Leeds, LS2 9JT (UK).
[e]   Dr. M. Yamada, Dr. N. Yoshinari, Prof. T. Konno,
        Prof. M. A. Halcrow
        Department of Chemistry, Graduate School of Science, Osaka
        University, Toyonaka, Osaka 560-0043 (Japan).
[f]   Dr. M. Yamada, current address:
        Division of Materials Science, Graduate School of Science and
        Technology, Nara Institute of Science and Technology, Ikoma, Nara
        630-0192 (Japan).

Introduction

Spin-crossover (SCO) compounds are metal/organic materials that switch between a high-spin and low-spin electronic configuration under a temperature, pressure or photochemical stimulus.[1-5] Structural and electronic changes accompanying an SCO event perturb many other properties of the compound, including its color, magnetic moment,[6] conductivity,[7] dielectric properties[8] and elastic moduli.[9] Recently proposed applications exploiting these properties of SCO materials[4,5] include their use as bits in electronic memory devices,[10] in micro-cantilevers[11] and for barocaloric refrigeration.[12] Most such applications require compounds exhibiting abrupt thermal SCO with significant thermal hysteresis, which are bistable at temperatures inside the hysteresis loop.[6] While examples with hysteresis widths of up to 140 K are known,[13] SCO materials showing hysteresis wider than 40 K are still unusual.[14-27] As a result, most SCO application studies are carried out with just two types of coordination polymer materials, with suitably hysteretic SCO that also spans room temperature.[28,29]

Studies of the structural basis underlying SCO hysteresis are hampered by challenges in structurally characterising such materials.[30] The intermolecular cooperativity required to induce SCO hysteresis is associated with a large structural modification during the transition, often (but not always[17,31]) involving a crystallographic phase change. Since that can lead to crystal decomposition, crystallographic data from such materials are often only available in one spin state. Other techniques including powder diffraction,[21,25] calorimetry[32] or EPR[33] can show the involvement of a phase change in hysteretic SCO, but without giving detailed structural insight.[34]

Some years ago, we reported that [FeL_2][BF$_4$]$_2$ (L = 2,6-*bis*-[5-methyl-1*H*-pyrazol-3-yl]pyridine; **1Fe**, Scheme 1) can be crystallized in anhydrous (phase A) or dihydrate crystal forms.[21] Crystalline **1Fe**·2H$_2$O contains a 1:1 mixture of low- and high-spin molecules between 5-300 K, but is readily dehydrated to a fully high-spin material upon heating to 350 K. The annealed sample (phase B) is distinct from the as-prepared anhydrous phase A, and evidently transforms sequentially to phases C and D on recooling from 350 K to just below room temperature. Further cooling of phase D leads to an abrupt spin-transition at $T_{1/2}$ = 205 K, which exhibits a 65 K thermal hysteresis loop in freshly prepared material although this narrows upon repeated thermal cycling (Figure S1). Since the low-spin phase E is distinct from phases A-D, this SCO is accompanied by yet another crystallographic phase change.[21]

Scheme 1. The complexes referred to in this work.

M = Fe, **1Fe**
M = Cu, **1Cu**
M = Zn, **1Zn**
M = Fe$_{0.97}$Cu$_{0.03}$, **1Fe,Cu**

Interestingly, the corresponding perchlorate salt [FeL_2][ClO$_4$]$_2$·2H$_2$O exhibits different spin-state properties. Dehydration of this salt leads to high-spin phase B, which transforms to phase C just above room temperature as before.[35] However, no further phase changes are observed at lower temperature for this material, which remains high-spin above 5 K.

The phase behavior of these anhydrous materials was analysed by powder diffraction, since single crystals of both hydrated salts degrade irreversibly upon dehydration. While their various phase changes were detected by this method, the structural basis underlying this complicated behavior was not elucidated. To address that, we have now examined [CuL_2][BF$_4$]$_2$·2H$_2$O (**1Cu**·2H$_2$O, Scheme 1) and [ZnL_2][BF$_4$]$_2$·2H$_2$O (**1Zn**·2H$_2$O), whose crystals are more robust to thermal cycling since they do not undergo spin state changes. These compounds have shed new light on the transformations undergone by **1Fe**, while also showing unexpected differences between themselves.

Results and Discussion

Treatment of L[36] with 0.5 equiv of the appropriate hydrated M[BF$_4$]$_2$ salt (M = Fe, Cu or Zn) in methanol yielded **1Fe**,[21] **1Cu** and **1Zn** following the usual work-up. While our original report synthesized crystalline **1Fe**·2H$_2$O by slow recrystallization from methanol solution, we have since found that to be an unreliable method for preparation of this phase. Hence, in this study, **1Fe**·2H$_2$O, **1Cu**·2H$_2$O and **1Zn**·2H$_2$O were all obtained by recrystallization of the crude complexes from hot water. This method usually gave polycrystalline material when the hot solutions were recooled, but sometimes yielded single crystals if the cooling was done sufficiently slowly. The dihydrate formulations of these compounds were confirmed by microanalysis and by TGA, which showed a clean mass loss equivalent to 2 equiv H$_2$O at 100 °C (**1Fe** and **1Cu**) or 120 °C (**1Zn**; Figure S2).

Although they are closely related, none of the three dihydrate compounds is perfectly isostructural (Figure 1). Crystalline **1Fe**·2H$_2$O (tetragonal, space group $I4_1/a$, $Z = 8$) contains an asymmetric unit with two unique complex cations, each with crystallographic $\bar{4}$ symmetry.[21] One cation is high-spin and donates hydrogen bonds to four BF$_4^-$ ions in the lattice through its ligand N–H groups, while the other is low-spin and donates four N–H...O hydrogen bonds to lattice water molecules. Crystals of **1Cu**·2H$_2$O (tetragonal, $I4_1/a$, $Z = 8$) have the same unit cell and space group as the iron complex, but now with just one unique cation environment lying on a C_2 symmetry axis. The [CuL_2]$^{2+}$ cations in this crystal each form two N–H...O and two N–H...F hydrogen bonds, with the latter being donated by the pyrazolyl donors along the complex's Jahn-Teller elongation axis. The unit cell of **1Zn**·2H$_2$O (tetragonal, $P4_2/n$, $Z = 2$) is related to the other compounds as $a\{Zn\} \approx a\{Fe/Cu\}/\sqrt{2}$ and $c\{Zn\} \approx c\{Fe/Cu\}/2$. The asymmetric unit of the zinc complex contains one unique cation on a $\bar{4}$ crystallographic site, with half a BF$_4^-$ ion and half a water molecule occupying the same region of the lattice near a crystallographic C_2 axis. Hence, each [ZnL_2]$^{2+}$

Figure 1. The asymmetric units of **1Fe**·2H$_2$O (left),[21] **1Cu**·2H$_2$O (center) and **1Zn**·2H$_2$O (right). Only the major orientations are shown of the disordered BF$_4^-$ ion in **1Cu**·2H$_2$O, and the disordered half-anion in **1Zn**·2H$_2$O, but both disorder sites of the water half-molecule are shown in the zinc complex. Water H atoms are not included in the crystallographic refinement of **1Zn**·2H$_2$O. C-bound H atoms have been omitted for clarity, and displacement ellipsoids are at the 50 % probability level. Color code: C, white; H, pale grey; B, pink; F, cyan; N, blue; O, red; Cu, Fe or Zn, green.

Figure 2. Packing diagrams of **1Cu**·2H$_2$O parallel to the (00-1) crystal plane (left); phase B of **1Cu** parallel to (001) (center); and phase C', parallel to (010) with the *c* axis horizontal (right). Only one orientation of each disordered BF$_4^-$ ion or half-ion is shown, but both components of the anion disorder about a C_2 axis in phase B are included. All atoms have arbitrary radii, with the complex cations de-emphasized for clarity. Other details as for Figure 1. The packing of **1Fe**·2H$_2$O is visually indistinguishable from **1Cu**·2H$_2$O in this view (Figure S4).

Figure 3. Packing diagrams of **1Zn**·2H$_2$O (left) and phases B (center) and C (right) of **1Zn**, each parallel to (001). Details as in Figures 1 and 2.

molecule forms an equal number of N–H...O and N–H...F hydrogen bonds, which are however randomly disordered in the lattice.
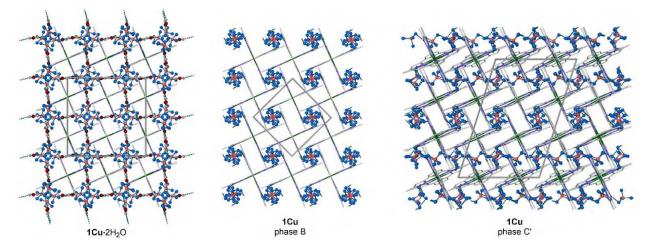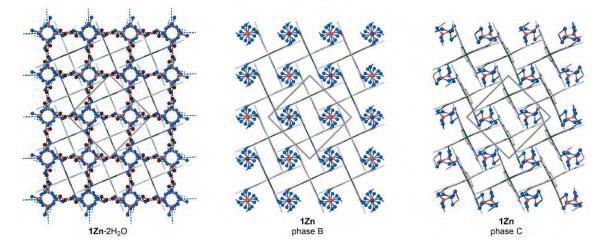
The crystal packing of all the compounds is based on the 'terpyridine embrace' motif, with four-fold layers of cations in the (001) crystal plane which interdigitate through their pyrazolyl arms (Figures 2 and 3).[37] Overlapping pyrazolyl groups on neighboring cations in each structure are separated by 3.5-3.6 Å, which corresponds to a Van der Waals contact rather than an attractive $\pi...\pi$ interaction.[38] That may reflect the steric influence of the ligand methyl substituents. However, the cations interact through intermolecular C−H...π contacts, between their methyl substituents and a pyrazolyl N–H N atom on their nearest neighbors within the layers (C...N = 3.2-3.5 Å; Table S9).

The cation layers are separated by hydrogen bonded chains of BF$_4^-$ and OH$_2$ molecules along the *a* and *b* directions, which propagate down *c* via alternating left- and right-handed 4$_1$ screw axes (Figure 2). The crystals differ in that the unit cell origin and

complex cation positions in **1Cu**·2H$_2$O are offset by $^a/_2$ compared to **1Fe**·2H$_2$O. As a consequence, each 4$_1$ axis is of opposite handedness in the iron and copper crystals, relative to the cation layers. That inverts the orientation of nearest neighbor BF$_4^-$/OH$_2$ chains generated by the screw along the *c* direction, thus presenting a different pattern of hydrogen bond acceptors to each cation in the two compounds (Figures S4-S6). The orientation of the cations in **1Zn**·2H$_2$O is similar to **1Cu**·2H$_2$O, but the BF$_4^-$/OH$_2$ chains in the zinc complex are disordered through the lattice (Figures 3 and S7).

A consistent trend between the crystals is that pyrazolyl groups involved in longer, high-spin Fe–N or Jahn-Teller-elongated Cu–N bonds hydrogen bond to the BF$_4^-$ ions, while pyrazolyl groups donating shorter low-spin Fe–N or basal Cu–N bonds interact with water molecules. Shorter, and stronger, metal–N bonds should polarise the adjacent N$^{\delta-}$–H$^{\delta+}$ groups to a greater extent, leading to a preference for the stronger hydrogen bond acceptor which is water in this case. The anion and water

disorder in **1Zn**·2H$_2$O thus reflects that all the metal–N bonds are equivalent in that compound, so separate N–H...O and N–H...F hydrogen bonding sites are not resolved.

The powder patterns of **1Fe**·2H$_2$O and **1Cu**·2H$_2$O are almost identical, but clearly different from **1Zn**·2H$_2$O. However, all three compounds transform to the same anhydrous phase B, when annealed at 350 K inside the diffractometer (Figure S8). The dehydration is accompanied by color changes from brown to yellow in **1Fe**, and from turquoise to green in **1Cu**, which are obvious to the naked eye. However, all the anhydrous materials reabsorb atmospheric moisture under ambient conditions over a period of *ca* 1 hr to regenerate the hydrated compounds. Hence, they are best generated *in situ* for physical characterization.

In contrast to **1Fe**·2H$_2$O, dehydration of **1Cu**·2H$_2$O and **1Zn**·2H$_2$O proceeds in single-crystal-to-single-crystal fashion. Phase B of both compounds (tetragonal, $P4_2/n$, $Z = 2$) closely resembles **1Zn**·2H$_2$O, although the half-water molecule in the asymmetric unit is absent (Figures 2, 3, S9 and S10). The BF$_4^-$ half-anion is disordered into the empty water site across a crystallographic C_2 axis, with each disorder site accepting just one hydrogen bond from a different cation (Figure S11). Hence, on average, each cation in phase B forms just two N–H...F hydrogen bonds in a random distribution through the crystal. This is also reflected in disorder of the Jahn-Teller elongation in **1Cu** (phase B), about the $\bar{4}$ special position occupied by the complex molecule. The *L* ligands in both phase B structures have a slightly *S*-shaped conformation, which is not present in the hydrated crystals. This has little effect on the dimensions of their terpyridine embrace layers, however (Table S10).

Although dehydration of **1Zn**·2H$_2$O does not change its crystallographic symmetry, dehydration of the crystals was confirmed by observation of the phase B→C transition on cooling (see below), which is not exhibited by the hydrated material. The powder diffraction patterns of **1Zn**·2H$_2$O and **1Zn** (phase B) are also clearly distinct (Figure S8).

Both anhydrous crystals undergo a crystallographic phase change on cooling towards room temperature. The transformations are accompanied by a reversible, rotational twinning of the lattice, which was resolved to allow full structure refinements of the low temperature phases. Surprisingly, however, the low temperature phase is different in each case. Phase B of **1Cu** transforms at 275±25 K to a phase C' (monoclinic, $P2_1/c$, $Z = 12$), whose asymmetric unit contains three formula units of the compound (Figure 2). In contrast to phase B, the Jahn-Teller distortions of the three unique cations in phase C' are crystallographically ordered, in an antiferrodistortive (alternating) arrangement within the cation layers.[39,40] The phase transition is accompanied by canting of some cations in the layers (Table S10), and by translation of some anions along [001] (Figure 2). These displacements allow each BF$_4^-$ ion to hydrogen bond to two different cations, thus doubling the number of hydrogen bonds in the lattice compared to phase B. Both these factors will contribute to the thermodynamics of the phase B→C' transformation.

Phase C' was analysed at 150, 200 and 250 K. A small but consistent increase in the magnitude of the Jahn-Teller distortion in all three cations as the crystal is cooled may reflect freezing out of residual Jahn-Teller disorder.[41] This is also apparent in its X- and Q-band powder EPR spectra, which are consistent with a disordered Jahn-Teller structure at 250 K but evolve towards a static lineshape between 200 and 100 K (Figures S14-S17).[40-42]

There are no other significant differences in the cation structures or anion disorder at the three temperatures.

In contrast, phase B of **1Zn** transforms at 295±10 K to a different structure, phase C (triclinic, $P\bar{1}$, $Z = 2$), which has just one unique molecule on a general crystallographic site (Figure 3). As for the copper compound, the molecules in this low temperature phase are positioned to maximize the number of N–H...F hydrogen bonds in the lattice. However, in contrast to **1Cu**, this is not achieved by significant molecular displacements in the lattice. Rather, the phase B→C transition in **1Zn** reflects a relaxation of the metal coordination sphere from the crystallographically imposed D_{2d} symmetry in phase B. This distortion is reflected in the *trans*-N{pyridyl}–Zn–N{pyridyl} angle (ϕ) which is 180° in phase B but decreases steadily in phase C as the crystal is cooled, to 173.21(8) (285 K), 169.88(7) (240 K) and 167.62(7)° (150 K). This is mostly accounted for by a rotation of one ligand [N(20)-C(37) in Figure S19] about an axis perpendicular to the other ligand, which remains relatively static over this temperature range (Figure 4). The twisting of the coordination geometry is also evident in the crystal α and β unit cell angles, which become more acute at lower temperatures (Figure S21). This is in turn reflected in the powder diffraction data from the compound (see below).

Figure 4. Overlays of the [Zn*L*$_2$]$^{2+}$ cation in phase C of **1Zn** at 285 (white), 240 (pink) and 150 K (purple), showing the temperature dependence of its molecular structure.

Twisted coordination geometries of the type seen in phase C are well known in complexes of tridentate ligands related to *L*, including other dipyrazolylpyridine (bpp) derivatives.[43,44] They are most common in high-spin iron(II) complexes, but are also found with zinc(II)[45,46] and other metal ions.[46,47] Notably the other published salt of [Zn*L*$_2$]$^{2+}$, [Zn*L*$_2$][Zn(Hpdc)$_3$]$_2$ (H$_2$pdc = 2,5-pyridinedicarboxylic acid), exhibits a comparable geometry to phase C with ϕ = 173.6(3)° at room temperature.[48] However, to our knowledge, this is the first observation of a significant temperature dependence in such a distortion. The structural changes are probably induced by the local lattice pressure about the complex molecule, during anisotropic contraction of the triclinic crystal on cooling.

The structural changes occurring upon dehydration of **1Fe**·2H$_2$O, **1Cu**·2H$_2$O and **1Zn**·2H$_2$O were monitored by synchrotron X-ray powder diffraction data. All three compounds were phase pure at the beginning of the experiment, and transformed cleanly to phase B upon heating *in situ* to 432 K. The powder pattern of **1Cu** was essentially unchanged upon subsequent cooling from 432 to 89 K (Figure S22). This was confirmed in a repeat experiment, using a laboratory powder diffractometer with Cu-K_α radiation (Figure S23). Unexpectedly, however, the simulated powder patterns predicted for phases B and C' of **1Cu** are almost identical, which makes it difficult to detect their interconversion by that technique (Figure S24).

In contrast, variable temperature powder diffraction data from **1Fe** and **1Zn** showed a phase B→C transition at 306±5 K (**1Fe**) and 295±10 K (**1Zn**) (Figures S25-S28). Interestingly **1Zn** contained an approximately 1:1 mixture of phases B and C below that temperature, implying only a fraction of that sample underwent the phase change (Figures 5 and S29); a weak feature at $2\theta = 6.8°$ arising from trace phase B is also evident in **1Fe** at these temperatures. Given the significant structural rearrangement involved in the transformation, we tentatively suggest a fraction of the sample might be kinetically trapped in phase B under the relatively rapid cooling employed in the synchrotron. Be that as it may, the powder pattern of phase C evolves significantly as the samples are cooled further until, for **1Fe** only, another phase transition occurs at 187±11 K (cooling) and 231±11 K (warming) corresponding to the SCO event. The other changes in the powder patterns were fully reversible upon rewarming to room temperature. The data for **1Fe** are consistent with our previous, lower resolution powder diffraction study of that compound with Cu-K_α radiation.[21]

The temperature dependence of the powder patterns of phase C for **1Fe** and **1Zn** is well-reproduced by simulations based on the crystal structures of **1Zn** at different temperatures (Figure 5). Hence the changes that we previously ascribed to an additional transformation to a putative 'phase D',[21] in fact arise from the evolution of the molecular structure in phase C as the crystal is cooled. Although the correspondence isn't perfect, the low-spin phase E powder pattern of **1Fe** shows similarities to phase C' of **1Cu**, implying those phases might be related (Figure S30). This is discussed further below.

The temperatures of the phase B→C transformations were confirmed by DSC measurements (Figures S31 and S32). Following a strong initial endotherm on heating corresponding to

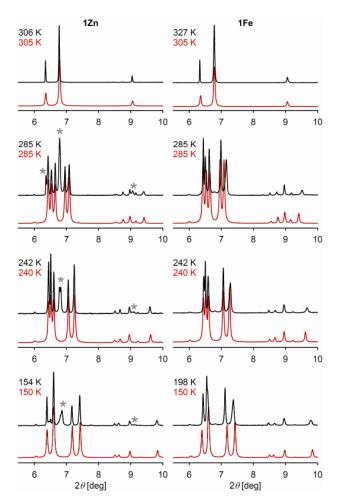**Figure 5.** Observed (black) and simulated (red) synchrotron powder diffraction data for phases B and C of **1Zn** and **1Fe**, at the temperatures indicated, The simulations for **1Fe** are based on the crystallographic models for **1Zn**, with the Zn atom replaced by Fe. The starred peaks originate from phase B of **1Zn**, and imply the low temperature **1Zn** sample is a mixture of the B and C phases.

the loss of lattice water, each **1M**·2H$_2$O material exhibits a reversible feature ascribable to the phase change at 303 (M = Fe), 251 (M = Cu) and 290 K (Zn). These are in good agreement with the single crystal and powder diffraction data. All the transitions show some thermal hysteresis, which can be attributed to the rapid 10 Kmin^{-1} temperature scan employed in the measurements. However, this hysteresis was *ca* 3.5x wider for the **1Cu** than for the other two materials. Since the phase B→C' transition temperature could not be confirmed in that compound by powder diffraction (see above), the significance of that observation is unclear. No other features were present in these data above 203 K, the lowest temperature accessible with our calorimeter.

Doping iron(II) spin-crossover materials with small quantities of isomorphous copper(II) dopants can provide a sensitive EPR spectroscopic probe of structural changes during spin-crossover events.[49-51] With that in mind, a mixed-metal sample [Fe$_x$Cu$_{1-x}L_2$][BF$_4$]$_2$·2H$_2$O (**1Fe,Cu**·2H$_2$O; $x \approx 0.97$) was prepared by co-crystallising the appropriate ratio of pre-formed **1Fe** and **1Cu** from hot water, as before. Magnetic measurements, TGA

and DSC data confirmed the composition and spin state behaviors of **1Fe,Cu**·2H$_2$O and anhydrous **1Fe,Cu** are identical to the parent iron compounds (Figures S2, S31 and S33).

The X-band EPR spectrum of as-prepared **1Fe,Cu**·2H$_2$O is invariant between 120-300 K, apart from some line-broadening at higher temperatures. It has an "inverse" axial lineshape[40,41,52] with resolved $A\{^{63,65}Cu\}$ hyperfine coupling, which resembles that of another Cu-doped [Fe$_y$Cu$_{1-y}$(bpp)$_2$][BF$_4$]$_2$ material at these temperatures (Figure S34).[50] The EPR spectrum of phase B of **1Fe,Cu** was not achieved, since data could only be measured at $T \leq 300$ K. Between 300-200 K, the spectrum of phase C shows a single rhombic Cu(II) dopant environment. However at 150 and 100 K, where the host lattice is low-spin, two Cu sites are resolved in the parallel region of the spectrum. These cation environments are best modelled in a 2:1 intensity ratio in the EPR simulation (Figures 6 and S35).[52]
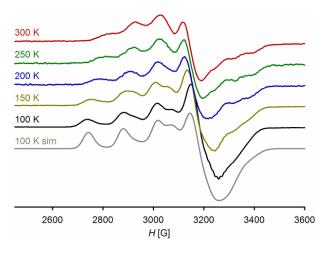

Figure 6. X-band EPR spectra of high-spin phase C ($T = 200$-300 K) and low-spin phase E (100-150 K) of anhydrous **1Fe,Cu**. A simulation of the 100 K spectrum is also shown; simulations at other temperatures are in Figure S34.

Conclusions

While they are all based on the same lattice type, the structural chemistry of **1Fe**·2H$_2$O, **1Cu**·2H$_2$O and **1Zn**·2H$_2$O is unexpectedly complicated. The freshly prepared hydrate crystals exhibit the same 'terpyridine embrace' motif of cation packing, but surrounded by differently oriented or disordered 2D networks of hydrogen-bonded anions and lattice water. The differences reflect that the lattice water is always positioned to accept a hydrogen bond from pyrazolyl donors forming shorter Fe–N or Cu–N bonds in those complexes. In **1Zn**·2H$_2$O, where all Zn–N{pyrazolyl} bonds are the same length, the anion and water sites are disordered.

All three compounds form the same anhydrous phase B upon annealing, but behave differently on recooling. Both **1Fe** and **1Zn** transform to the same triclinic phase (phase C) close to room temperature. However, **1Cu** instead forms a different, monoclinic phase at around 250 K. We attribute the difference to the stereochemical consequences of the Jahn-Teller distortion in **1Cu**, which is not show by the iron or zinc compounds.

These results have led to a new understanding of **1Fe**·2H$_2$O, which undergoes a thermal spin transition with a 65 K thermal

hysteresis loop after *in situ* dehydration (Figure 7).[21] Our original powder diffraction study of **1Fe** showed a clear phase change just above room temperature, that we labelled phase B→C. Both these phases have now been structurally characterized in **1Zn**. We also attributed further changes to its powder diffraction between 293 and 240 K to another transformation, from phase C to a putative phase D.[21] However, phase C in **1Zn** is strikingly temperature-dependent since its coordination geometry becomes steadily more twisted, and its unit cell more canted, as the temperature decreases. The temperature-dependent powder patterns of **1Fe** between 285 and 198 K, and of **1Zn** between 285 and 154 K, are fully reproduced by simulations based on phase C of the zinc complex. That is, by the evolution of phase C on cooling (Figures 4 and S17). Hence, our previous proposal of an additional intermediate high-spin phase D in this system was incorrect (Figure S1).
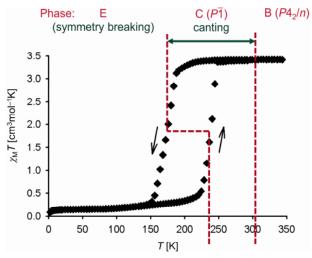

Figure 7. Relationship between the crystallographic phases and magnetic behavior of **1Fe**, from the results of this study. The labelling of the phases is the same as in our original report, for consistency (Figure S1).[21]

The identity of the low-spin phase E of **1Fe** is still not proven. However similarities of its powder pattern with phase C' of **1Cu**, and its 2:1 ratio of cation sites detected by EPR (Figure 6), are both circumstantially consistent with a tripling of the asymmetric unit during the phase C→E transformation. Hence, even if they are not perfectly isostructural, we propose phase E and phase C' are crystallographically related.

Distorted molecular structures with reduced values of ϕ, as in phase C, are common in high-spin complexes of the [Fe(bpp)$_2$]$^{2+}$ type.[42,43] They reflect an angular Jahn-Teller distortion of the high-spin ^5T configuration and, as such, are a property of the high-spin state. However, this is the first time a temperature-dependence of the ϕ distortion has been observed, since it was first defined 18 years ago.[53] That has consequences for structure:function analyses of SCO in these compounds,[30,54] where crystallographic comparison of the spin states may only be meaningful if they are measured close to the SCO transition temperature.

6

Significant changes in ϕ between the high- and low-spin states of a material can lead to highly cooperative SCO, which is likely to contribute to the thermal hysteresis in **1Fe**.[27,55] However, high-spin materials that deviate too strongly from the D_{2d} symmetry preferred by the low-spin form, are kinetically trapped in their high-spin state and so are inactive to SCO.[43,53,56] In that respect, it is counterintuitive that the increased distortions in phase C of **1Fe** at lower temperatures eventually lead to SCO; but, phase C in the corresponding perchlorate salt $[FeL_2][ClO_4]_2$ does not evolve with temperature by powder diffraction, and no SCO occurs.[35] This apparent anomaly is under investigation.

Experimental Section

Instrumentation

Elemental microanalyses were performed by the microanalytical services at the University of Leeds and London Metropolitan University. ^1H NMR spectra employed a Bruker DPX300 spectrometer operating at 300.1 MHz. Magnetic susceptibility measurements were performed on a Quantum Design SQUID or SQUID/VSM magnetometer, with an applied field of 5000 G and a scan rate of 5 $Kmin^{-1}$. A diamagnetic correction for the sample was estimated from Pascal's constants;[57] a previously measured diamagnetic correction for the sample holder was also applied.

Thermogravimetric analyses (TGAs) were obtained with a TA Instruments TGA Q50 analyser heating at a rate of 10 K min^{-1}under a stream of nitrogen gas, while differential scanning calorimetry (DSC) used a TA Instruments DSC Q20 calorimeter, also with a temperature ramp of 10 $Kmin^{-1}$. X-ray powder diffraction data were obtained with a Bruker D8 Advance A25 diffractometer using Cu-K_α radiation (λ = 1.5418 Å), or at beamline BL02B2 of the SPring-8 synchrotron equipped with MYTHEN X-ray detectors (λ = 1.000414(2) Å).[58] X- and Q-band EPR spectra were recorded on a Bruker EMX spectrometer, and EPR spectral simulations were performed using *EasySpin*.[59]

Materials and methods

2,6-*Bis*-[5-methyl-1H-pyrazol-3-yl]pyridine (L)[36] and $[FeL_2][BF_4]_2$ (**1Fe**)[21] were prepared by the literature procedures.

Synthesis of $[FeL_2][BF_4]_2$·$2H_2O$ (1Fe·$2H_2O$). Pre-formed **1Fe** (0.5 g) was dissolved in hot water (75 cm^3), which yielded an orange-brown solution when the temperature reached *ca* 80 °C. After a hot filtration, the solution was allowed to cool to room temperature under ambient conditions, yielding a brown microcrystalline precipitate of **1Fe**·$2H_2O$. This was collected and dried over P_2O_5, at ambient temperature and pressure. Elemental analysis calcd (%) for $C_{26}H_{26}B_2F_8FeN_{10}$·$2H_2O$ C 42.0, H 4.06, N 18.8; found C 41.9, H 3.86, N 18.7. Other analytical data from this product are identical to those previously published for this material.[21]

[**1Fe**·$2H_2O$ cannot be prepared directly by treating Fe[BF$_4$]$_2$·$6H_2O$ with 2 equiv L in aqueous solution, because the organic ligand L is insufficiently water soluble].

Synthesis of $[CuL_2][BF_4]_2$·$2H_2O$ (1Cu·$2H_2O$). A solution of L (0.5 g, 2.1 mmol) and Cu[BF$_4$]$_2$·$4H_2O$ (0.32 g, 1.1 mmol) in MeOH (50 cm^3) was stirred until all the solid had dissolved. The resultant solution was filtered, and concentrated to *ca*. 5 cm^3. Addition of excess diethyl ether afforded the complex as a blue-green precipitate. This was recrystallized from hot water, as described above, to yield **1Cu**·$2H_2O$ as a turquoise microcrystalline solid. Yield 0.26 g, 68 %. Elemental analysis calcd (%)

for $C_{26}H_{26}B_2CuF_8N_{10}$·$2H_2O$ C 41.5, H 4.02, N 18.6; found C 41.7, H 4.00, N 18.7.

Synthesis of $[ZnL_2][BF_4]_2$·$2H_2O$ (1Zn·$2H_2O$). Method as for **1Cu**·$2H_2O$, using Zn[BF$_4$]$_2$·$6H_2O$ (0.36 g, 1.1 mmol). The crude complex is less water soluble that the other two compounds, so a larger volume of hot water (*ca* 100 cm^3) is required for the recrystallization. The dihydrate product is a white microcrystalline solid. Yield 0.26 g, 68 %. ^1H NMR [CD$_3$NO$_2$] δ 2.28 (12H, CH_3), 6.90 (4H, Pz H^4), 8.14 (d, 8.9 Hz, 4H, Py $H^{\beta/5}$), 8.47 (t, 8.9 Hz, 2H, Py H^4), 11.13 (br s, 4H, Pz NH); elemental analysis calcd (%) for $C_{26}H_{26}B_2F_8N_{10}Zn$·$2H_2O$ C 41.4, H 4.01, N 18.6; found C 41.7, H 3.90, N 18.7.

Synthesis of $[Fe_{0.97}Cu_{0.03}L_2][BF_4]_2$·$2H_2O$ (1Fe,Cu·$2H_2O$). A mixture of **1Fe** (0.50 g) and **1Cu** (0.015 g) was recrystallized from hot water as above, taking care that all the solid had dissolved before the solution was filtered. The product was a brown microcrystalline solid, which was visually indistinguishable from the pure iron compound. Yield 0.26 g, 68 %. Elemental analysis calcd (%) for $C_{26}H_{26}B_2Cu_{0.03}F_8Fe_{0.97}N_{10}$·$2H_2O$ C 42.0, H 4.06, N 18.8; found C 42.1, H 3.95, N 18.7.

Single Crystal Structure Analyses

Small plate-like crystals of **1Cu**·$2H_2O$ and **1Zn**·$2H_2O$ were obtained by recrystallization from hot water as before, but using more dilute solutions (*ca* 0.2 g in 50 cm^3) and with controlled slow cooling of the solutions using an oil bath. All data collections for the different phases of each compound were collected using the same crystal. All diffraction data were collected with an Agilent Supernova dual-source diffractometer using monochromated Cu-K_α radiation (λ = 1.54184 Å). The diffractometer is fitted with an Oxford Cryostream low-temperature devices. All the structures were solved by direct methods (*SHELXS97*[60]), and developed by full least-squares refinement on F^2 (*SHELXL97*[60]). Crystallographic figures were prepared using *XSEED*.[61] Experimental data from the structure determinations and descriptions of the crystallographic refinements are included in the Supporting Information.

CCDC-1973368 and 1973389-1973398 contain the supplementary crystallographic data for this paper. Codes for the individual structures are listed in the Supporting Information. These data can be obtained free of charge from The Cambridge Crystallographic Data Center via www.ccdc.cam.ac.uk/data_request/cif.

[1]   M. A. Halcrow (ed), *Spin-crossover materials – properties and applications,* John Wiley & Sons, Chichester, UK, 2013, p. 568.

[2] J. Zarembowitch, F. Varret, A. Hauser, J. A. Real, K. Boukheddaden, *C. R. Chimie* **2018**, *21*, 1056–1059.

[3] O. Sato, *Nature Chem.* **2016**, *8*, 644–656.

[4] K. S. Kumar, M. Ruben, *Coord. Chem. Rev.* **2017**, *346*, 176–205.

[5] S. Rat, M. Piedrahita-Bello, L. Salmon, G. Molnár, P. Demont, A. Bousseksou, *Adv. Mater.* **2018**, *30*, 17003862.

[6] O. Kahn, J. Krõber, C. Jay, *Adv. Mater.* **1992**, *4*, 718–728.

[7] See *eg* a) A. Rotaru, I. A. Gural'skiy, *Chem. Commun.* **2012**, 48, 4163–4165; b) H. Phan, S. M. Benjamin, E. Steven, J. S. Brooks, M. Shatruk, *Angew. Chem. Int. Ed.* **2015**, *54*, 823–827; *Angew. Chem.* **2015**, *127*, 837–841; c) H.-Y. Wang, J.-Y. Ge, C. Hua, C.-Q. Jiao, Y. Wu, C. F. Leong, D. M. D'Alessandro, T. Liu, J.-L. Zuo*, Angew. Chem. Int. Ed.* **2017**, *56*, 5465–5470; *Angew. Chem.* **2017**, *129*, 5557–5562.

[8] See *eg* a) H. Zheng, Y.-S. Meng, G.-L. Zhou, C.-Y. Duan, O. Sato, S. Hayami, Y. Luo, T. Liu, *Angew. Chem. Int. Ed.* **2018**, *57*, 8468–8472; *Angew. Chem.* **2018**, *130*, 8604–8608; b) S. Rat, M. Piedrahita-Bello, L. Salmon, G. Molnár, P. Demont, A. Bousseksou, *Adv. Mater.* **2018**, *30*, 1705275.

[9] M. Mikolasek, M. D. Manrique-Juárez, H. J. Shepherd, K. Ridier, S. Rat, V. Shalabaeva, A.-C. Bas, I. E. Collings, F. Mathieu, J. Cacheux, T. Leïchlé, L. Nicu, W. Nicolazzi, L. Salmon, G. Molnár, A. Bousseksou, *J. Am. Chem. Soc.* **2018**, *140*, 8970–8979.

[10] a) C. Lefter, S. Rat, J. S. Costa, M. D. Manrique-Juárez, C. M. Quintero, L. Salmon, I. Séguy, T. Leichle, L. Nicu, P. Demont, A. Rotaru, G. Molnár, A. Bousseksou, *Adv. Mater.* **2016**, *28*, 7508–7514; b) R. Torres-Cavanillas, R. Sanchis-Gual, J. Dugay, M. Coronado-Puchau, M. Giménez-Marqués, E. Coronado, *Adv. Mater.* **2019**, *31*, 1900039.

[11] a) M. D. Manrique-Juárez, S. Rat, L. Salmon, G. Molnár, C. M. Quintero, L. Nicu, H. J. Shepherd, A. Bousseksou, *Coord. Chem. Rev.* **2016**, *308*, 395–408; b) M. D. Manrique-Juárez, F. Mathieu, V. Shalabaeva, J. Cacheux, S. Rat, L. Nicu, T. Leïchlé, L. Salmon, G. Molnár, A. Bousseksou, *Angew. Chem. Int. Ed.* **2017**, *56*, 8074–8078; *Angew. Chem.* **2017**, *129*, 8186–8190.

[12] a) P. J. von Ranke, B. P. Alho, R. M. Ribas, E. P. Nobrega, A. Caldas, V. S. R. de Sousa, M. V. Colaço, L. F. Marques, D. L. Rocco, P. O. Ribeiro, *Phys. Rev. B* **2018**, *98*, 224408; b) S. P. Vallone, A. N. Tantillo, A. M. dos Santos, J. Molaison, R. Kulmaczewski, A. Chapoy, P. Ahmadi, M. A. Halcrow, K. G. Sandeman, *Adv. Mater.* **2019**, *31*, 1807334.

[13] M. A. Halcrow, *Chem. Lett.* **2014**, *43,* 1178–1188.

[14] E. König, G. Ritter, S. K. Kulshreshtha, N. Csatary, *Inorg. Chem.* **1984**, *23*, 1903–1910.

[15] T. Buchen, P. Gütlich, K. H. Sugiyarto, H. A. Goodwin, *Chem. Eur. J.* **1996**, *2*, 1134–1138.

[16] J.-F. Létard, P. Guionneau, E. Codjovi, O. Lavastre, G. Bravic, D. Chasseau, O. Kahn, *J. Am. Chem. Soc.* **1997**, *119*, 10861–10862.

[17] a) Z. J. Zhong, J.-Q. Tao, Z. Yu, C.-Y. Dun, Y.-J. Liu, X.-Z. You, *J. Chem. Soc. Dalton Trans.* **1998**, 327–328; b) H. J. Shepherd, T. Palamarciuc, P. Rosa, P. Guionneau, G. Molnár, J.-F. Létard, A. Bousseksou, *Angew. Chem. Int. Ed.* **2012**, *51*, 3910–3914; *Angew. Chem.* **2012**, *124*, 3976–3980.

[18] a) B. Weber, W. Bauer, J. Obel, *Angew. Chem. Int. Ed.* **2008**, *47*, 10098–10101; *Angew. Chem.* **2008**, *120*, 10252–10255; b) B. Weber, W. Bauer, T. Pfaffeneder, M. M. Dîrtu, A. D. Naik, A. Rotaru, Y. Garcia, *Eur. J. Inorg. Chem.* **2011**, 3193–3206.

[19] S. Hayami, Z.-Z. Gu, H. Yoshiki, A. Fujishima, O. Sato, *J. Am. Chem. Soc.* **2001**, *123*, 11644–11650; S. Hayami, K. Hiki, T. Kawahara, Y. Maeda, D. Urakami, K. Inoue, M. Ohama, S. Kawata, O. Sato, *Chem. Eur. J.* **2009**, *15*, 3497–3508.

[20] M. Nihei, M. Tahira, N. Takahashi, Y. Otake, Y. Yamamura, K. Saito, H. Oshio, *J. Am. Chem. Soc.* **2010**, *132*, 3553–3560.

[21] T. D. Roberts, F. Tuna, T. L. Malkin, C. A. Kilner, M. A. Halcrow, *Chem. Sci.* **2012**, *3*, 349–354.

[22] M. B. Bushuev, V. A. Daletsky, D. P. Pishchur, Y. V. Gatilov, I. V. Korolkov, E. B. Nikolaenkova, V. P. Krivopalov, *Dalton Trans.* **2014**, *43*, 3906–3910.

[23] S. Floquet, M.-L. Boillot, E. Rivière, F. Varret, K. Boukheddaden, D. Morinea, P. Négrier, *New J. Chem.* **2003**, *27*, 341.

[24] S. Kang, Y. Shiota, A. Kariyazaki, S. Kanegawa, K. Yoshizawa, O. Sato, *Chem. Eur. J.* **2016**, *22*, 532–538.

[25] W. Phonsri, P. Harding, L. Liu, S. G. Telfer, K. S. Murray, B. Moubaraki, T. M. Ross, G. N. L. Jameson, D. J. Harding, *Chem. Sci.* **2017**, *8*, 3949–3959.

[26] A. Djemel, O. Stefanczyk, M. Marchivie, E. Trzop, E. Collet, C. Desplanches, R. Delimi, G. Chastanet, *Chem. Eur. J.* **2018**, *24*, 14760–14767.

[27] K. S. Kumar, B. Heinrich, S. Vela, E. Moreno-Pineda, C. Bailly, M. Ruben, *Dalton Trans.* **2019**, *48*, 3825–3830.

[28] O. Roubeau, *Chem. Eur. J.* **2012**, *18*, 15230–15244; L. G. Lavrenova, O. G. Shakirova*, Eur. J. Inorg. Chem.* **2013**, 670–682.

[29] Z.-P. Ni, J.-L. Liu, M. N. Hoque, W. Liu, J.-Y. Li, Y.-C. Chen, M.-L. Tong, *Coord. Chem. Rev.* **2017**, *335*, 28–43.

[30] M. A. Halcrow, *Chem. Soc. Rev.* **2011**, *40*, 4119–4142.

[31] G. A. Craig, J. S. Costa, O. Roubeau, S. J. Teat, G. Aromí, *Chem. Eur. J.* **2011**, *17*, 3120–3127.

[32] T. Nakamoto, A. Bhattacharjee, M. Sorai, *Bull. Chem. Soc. Jpn.* **2004**, *77*, 921–932.

[33] R. C. W. Sung, B. R. McGarvey, *Inorg. Chem.* **1999**, *38*, 3644–3650.

[34] Mössbauer spectrum line widths are usually too broad to detect crystallographic symmetry breaking in iron SCO compounds above liquid helium temperatures. See refs [14,15,20,23,25] and the following additional examples: a) K. H. Sugiyarto, W.-A. McHale, D. C. Craig, A. D. Rae, M. L. Scudder, H. A. Goodwin, *Dalton Trans.* **2003**, 2443–2448; b) M. Yamada, H. Hagiwara, H. Torigoe, N. Matsumoto, M. Kojima, F. Dahan, J.-P. Tuchagues, N. Re, S. Iijima, *Chem. Eur. J.* **2006**, *12*, 4536–4549; c) A. Bhattacharjee, P. J. van Koningsbruggen, W. Hibbs, J. S. Miller, P. Gütlich, *J. Phys. Condens. Matter* **2007**, *19*, 406202; d) M. Griffin, S. Shakespeare, H. J. Shepherd, C. J. Harding, J.-F. Létard, C. Desplanches, A. E. Goeta, J. A. K. Howard, A. K. Powell, V. Mereacre, Y. Garcia, A. D. Naik, H. Müller-Bunz, G. G. Morgan, *Angew. Chem. Int. Ed.* **2011**, *50*, 896–900; *Angew. Chem.* **2011**, *123*, 926–930; e) H. Hang, B. Fei, X. Q. Chen, M. L. Tong, V. Ksenofontov, I. A. Gural'skiy, X. Bao, *J. Mater. Chem. C* **2018**, *6*, 3352–3361.

[35] T. D. Roberts, M. A. Little, F. Tuna, C. A. Kilner, M. A. Halcrow, *Chem. Commun.* **2013**, *49*, 6280–6282.

[36] Y. Zhou, W. Chen, D. Wang, *Dalton Trans.* **2008**, 1444–1453.

[37] I. Dance, M. Scudder, *CrystEngComm* **2009**, *11*, 2233–2247.

[38] a) C. A. Hunter, J. K. M. Sanders, *J. Am. Chem. Soc.* **1990**, *112*, 5525–5534; b) C. R. Martinez, B. L. Iverson, *Chem. Sci.* **2012**, *3*, 2191–2201.

[39] A similar three-fold expansion of the unit cell, driven by a Jahn-Teller order/disorder transition, occurs at much lower temperature in the stereochemically related complex [Cu(1-bpp)₂][BF₄]₂ (1-bpp = 2,6-di[pyrazol-1-yl]pyridine). M. A. Leech, N. K. Solanki, M. A. Halcrow, J. A. K. Howard, S. Dahaoui, *Chem. Commun.* **1999**, 2245–2246.

[40] M. A. Hitchman, *Comments Inorg. Chem.* **1994**, *15*, 197–254.

[41] a) B. Hathaway, M. Duggan, A. Murphy, J. Mullane, C. Power, A. Walsh, B. Walsh, *Coord. Chem. Rev.* **1981**, *36*, 267–324; b) L. R. Falvello, *J. Chem. Soc. Dalton Trans.* **1997**, 4463–4475.

[42] See *eg* a) P. Chaudhuri, K. Oder, K. Wieghardt, J. Weiss, J. Reedijk, W. Hinrichs, J. Wood, A. Ozarowski, H. Stratemaier, D. Reinen, *Inorg. Chem.* **1986**, *25*, 2951–2958; b) H. Stratemeier, B. Wagner, E. R. Krausz, R. Linder, H.-H. Schmidtke, J. Pebler, W. E. Hatfield, L. ter Haar, D. Reinen, M. A. Hitchman, *Inorg. Chem.* **1994**, *33*, 2320–2329; c) C. A. Kilner, E. J. L. McInnes, M. A. Leech, G. S. Beddard, J. A. K. Howard, F. E. Mabbs, D. Collison, A. J. Bridgeman, M. A. Halcrow, *Dalton Trans.* **2004**, 236–243; d) C. J. Simmons, H. Stratemeier, G. R. Hanson, M. A. Hitchman, *Inorg. Chem.* **2005**, *44*, 2753–2760.

[43] a) M. A. Halcrow, *Coord. Chem. Rev.* **2009**, *253*, 2493–2514; b) L. J. Kershaw Cook, R. Mohammed, G. Sherborne, T. D. Roberts, S. Alvarez, M. A. Halcrow, *Coord. Chem. Rev.* **2015**, *289–290*, 2–12.

[44] G. A. Craig, O. Roubeau, G. Aromí, *Coord. Chem. Rev.* **2014**, *269*, 13–31.

[45] See *eg* a) F. Dumitru, Y.-M. Legrand, A. Van der Lee, M. Barboiu, *Chem. Commun.* **2009**, 2667–2669; b) F. Dumitru, Y. M. Legrand, E.

Petit, A. Van der Lee, M. Barboiu, *Dalton Trans.* **2012**, *41*, 11860–11865;

[46] a) K. Pringouri, M. U. Anwar, L. Mansour, N. Doupnik, Y. Beldjoudi, E. L. Gavey, M. Pilkington, J. M. Rawson, *Dalton Trans.* **2018**, *47*, 15725–15736; b) K. E. Burrows, R. Kulmaczewski, O. Cespedes, S. A. Barrett, M. A. Halcrow, *Polyhedron* **2018**, *149*, 134–141.

[47] See *eg* a) C. W. Glynn, M. M. Turnbull, *Transition Met. Chem.* **2002**, *27*, 822–831; b) G. Stupka, L. Gremaud, G. Bernardinelli, A. F. Williams, *Dalton Trans.* **2004**, 407–412; c) H. Wu, X. Huang, J. Yuan, F. Kou, F. Jia, B. Liu, K. Wang, *Eur. J. Med. Chem.* **2010**, *45*, 5324–5330; d) Z.-Y. Ding, Y.-S. Meng, Y. Xiao, Y.-Q. Zhang, Y.-Y. Zhu, S. Gao, *Inorg. Chem. Front.* **2017**, *4*, 1909–1916; e) K. N. Lazarou, I. Stamatopoulos, V. Psycharis, C. Duboc, C. P. Raptopoulou, Y. Sanakis, *Polyhedron* **2018**, *155*, 291–301.

[48] Q.-L. Guan, Z. Liu, W.-J. Wei, Y.-H. Xing, J. Liu, R. Zhang, Y.-N. Hou, X. Wang, F.-Y. Bai, *New J. Chem.* **2014**, *38*, 3258–3268.

[49] a) A. Ozarowski, B. R. McGarvey, *Inorg. Chem.* **1989**, *28*, 2262–2266; b) P. J. Kunkeler, P. J. van Koningsbruggen, J. P. Cornelissen, A. N. van der Horst, A. M. van der Kraan, A. L. Spek, J. G. Haasnoot, J. Reedijk, *J. Am. Chem. Soc.* **1996**, *118*, 2190–2197.

[50] R. Docherty, F. Tuna, C. A. Kilner, E. J. L. McInnes, M. A. Halcrow, *Chem. Commun.* **2012**, *48*, 4055–4057.

[51] S. V. Tumanov, S. L. Veber, S. Greatorex, M. A. Halcrow, M. V. Fedin, *Inorg. Chem.* **2018**, *57*, 8709–8713.

[52] Samples could not be annealed above room temperature inside the EPR spectrometer, so **1Cu**·2H$_2$O and **1Fe,Cu**·2H$_2$O were dehydrated in an oven then transferred to the spectrometer for measurement. Since the anhydrous materials rapidly rehydrate upon cooling, measurements of those compounds were experimentally challenging. Spectra of **1Cu** were ultimately obtained at X-band and Q-band, after many attempts, but only X-band spectra of **1Fe,Cu** were achieved in the time available.

[53] J. M. Holland, J. A. McAllister, C. A. Kilner, M. Thornton-Pett, A. J. Bridgeman, M. A. Halcrow, *J. Chem. Soc. Dalton Trans.* **2002**, 548–554.

[54] M. A. Halcrow, I. Capel Berdiell, C. M. Pask, R. Kulmaczewski, *Inorg. Chem.* **2019**, *58*, 9811−9821.

[55] L. J. Kershaw Cook, F. L. Thorp-Greenwood, T. P. Comyn, O. Cespedes, G. Chastanet, M. A. Halcrow, *Inorg. Chem.* **2015**, *54*, 6319−6330.

[56] S. Vela, J. J. Novoa, J. Ribas-Arino, *Phys. Chem. Chem. Phys.* **2014**, *16*, 27012–27024.

[57] C. J. O'Connor, *Prog. Inorg. Chem.* **1982**, *29*, 203–283.

[58] S. Kawaguchi, M. Takemoto, K. Osaka, E. Nishibori, C. Moriyoshi, Y. Kubota, Y. Kuroiwa, K. Sugimoto, *Rev. Sci. Instrum.* **2017**, *88*, 08511.

[59] S. Stoll, A. Schweiger, *J. Magn. Reson.* **2006**, *178*, 42–55.

[60] G. M. Sheldrick, *Acta Cryst. Sect. A Found. Cryst.* **2008**, *64*, 112−122.

[61] L. J. Barbour, *J. Supramol. Chem.* **2001**, *1*, 189−191.